This is a postprint version of the following published document:

Available at https://doi.org/10.1021/acs.jpclett.0c02203

(Article begins on next page)

Thermodynamics of the Interaction between the Spike Protein of Severe Acute Respiratory Syndrome Coronavirus-2 and the Receptor of Human Angiotensin-Converting Enzyme 2. Effects of Possible Ligands

Cristina García-Iriepa, Cécilia Hognon, Antonio Francés-Monerris, Isabel Iriepa, Tom Miclot, Giampaolo Barone, Antonio Monari*, and Marco Marazzi*

Corresponding Authors

Marco Marazzi – Department of Analytical Chemistry, Physical Chemistry and Chemical Engineering and Chemical Research Institute "Andres M. del Ri ́o" (IQAR), Universidad de Alcala, 28871 Alcaláde Henares, Madrid, Spain; orcid.org/0000- 0001-7158-7994; Email: marco.marazzi@uah.es

Antonio Monari – Universitéde Lorraine and CNRS, LPCT UMR 7019, F-54000 Nancy, France; orcid.org/0000- 0001-9464-1463; Email: antonio.monari@univ-lorraine.fr

Authors

Cristina García-Iriepa – Department of Analytical Chemistry, Physical Chemistry and Chemical Engineering and Chemical Research Institute "Andres M. del Ri ́o" (IQAR), Universidad de Alcala, 28871 Alcala ́de Henares, Madrid, Spain; orcid.org/ 0000-0002-7577-8242

Cecilia Hognon ́– Universitéde Lorraine and CNRS, LPCT UMR 7019, F-54000 Nancy, France

Antonio Frances-Monerris ́– Universitéde Lorraine and CNRS, LPCT UMR 7019, F-54000 Nancy, France; Departament de Quimica Fi ́sica, Universitat de Valencia, 46100 ` Burjassot, Spain; orcid.org/0000-0001-8232-4989

Isabel Iriepa – Chemical Research Institute "Andres M. del Ri ́o" (IQAR) and Department of Organic and Inorganic Chemistry, Universidad de Alcala, 28871 Alcala ́de Henares, Madrid, Spain

Tom Miclot – Universitéde Lorraine and CNRS, LPCT UMR 7019, F-54000 Nancy, France; Department of Biological, Chemical and Pharmaceutical Sciences and Technologies, Universitàdegli Studi di Palermo, 90128 Palermo, Italy

Giampaolo Barone – Department of Biological, Chemical and Pharmaceutical Sciences and Technologies, Universitàdegli Studi di Palermo, 90128 Palermo, Italy; orcid.org/0000-0001-8773-2359

Abstract

Since the end of 2019, the coronavirus SARS-CoV-2 has caused more than 1000000 deaths all over the world and still lacks a medical treatment despite the attention of the whole scientific community. Human angiotensin-converting enzyme 2 (ACE2) was recently recognized as the transmembrane protein that serves as the point of entry of SARS-CoV-2 into cells, thus constituting the first biomolecular event leading to COVID-19 disease. Here, by means of a state-of-the-art computational approach, we propose a rational evaluation of the molecular mechanisms behind the formation of the protein complex. Moreover, the free energy of binding between ACE2 and the active receptor binding domain of the SARS-CoV-2 spike protein is evaluated quantitatively, providing for the first time the thermodynamics of virus–receptor recognition. Furthermore, the action of different ACE2 ligands is also examined in particular in their capacity to disrupt SARS-CoV-2 recognition, also providing via a free energy profile the quantification of the ligand-induced decreased affinity. These results improve our knowledge on molecular grounds of the SARS-CoV-2 infection and allow us to suggest rationales that could be useful for the subsequent wise molecular design for the treatment of COVID-19 cases.

A novel strain of coronavirus inducing severe acute respiratory disease (SARS) developed at the end of 2019 in mainland China and was later identified as SARS-CoV-2. Since then, after readily diffusing in eastern countries, SARS-CoV-2 has been at the origin of the outbreak of a severe pandemic of coronavirus disease-19 (COVID-19), at present widespread on all of the continents. (1−4) Strict social distancing and lock down measures have since been implemented to contain the diffusion of COVID-19 and the pressure it exerts on public health systems, due to the possible development of acute respiratory stress and bilateral pneumonia, requiring appropriate intensive care treatment. (5−7) Indeed, although the mortality ratio of COVID-19 is relatively low, compared to other related diseases, and usually associated with other preexistent morbidity, the very high transmissibility ratio, also due to a large number of asymptomatic patients, is related to the very fast growing rate of infection. (8−10) When this paper was being prepared, COVID-19 had infected more than 38.3 million persons worldwide, causing more than 1000000 deaths, and after having severely affected Asia and Europe is rapidly spreading across the whole world with the exception of Antarctica. (11) However, at present no real definitive therapeutic strategy is available to counteract SARS-CoV-2 infection.

Due to the unprecedented severity of the sanitary crisis, and its strong impact on both social and economic life, important scientific efforts have been devoted to modeling and comprehending the action of the virus and

the outcome of the infection. In particular, the genome of the virus has been rapidly sequenced, [12,13] and in parallel, the structure of its main protein apparatus has been resolved, [14−16] especially using cryogenic electron microscopy (cryoEM) techniques. [17] Molecular modeling and simulation studies have also been performed to rationalize, at the atomistic level, the behavior of the different involved proteins, [18] the pattern of interactions between them and other biological structures such as nucleic acids, [19] and the inherent differences between the SARS-CoV-2 proteome and those of other coronaviruses, such as SARS-CoV or the Middle East respiratory syndrome (MERS) agents. [20]

Among the varied protein apparatus of SARS-CoV-2, special attention has been devoted to the spike protein. This large protein includes a transmembrane domain protruding from the surface of the viral envelope, used by the virus to recognize the host cell. [21] Indeed, after its binding to the human receptors, via its specific receptor binding domain (RBD), the large conformational changes that are induced allow the fusion of the viral and host membranes, which represents the first step of the infection, i.e., the entry of the viral material into healthy cells. High-resolution structures of the full spike protein complex have been obtained, also resolving different conformational states of RBD, namely the active open conformations, the semiactive state, and the closed state. [17]

The molecular target of the spike protein of coronaviruses in general and SARS-CoV-2 in particular, their entry gate, has been recognized in angiotensin-converting enzyme 2 [ACE2 (Figure 1)]. [22] ACE2 is largely present in the external membranes of cells belonging to different human organs, such as the lungs, kidneys, and intestine, and plays a fundamental role in regulating blood pressure. [23,24] In addition, it plays a secondary role in regulating the membrane trafficking of neutral amino acid transporters. [25] The interaction with ACE2, and consequently the inhibition of its biological functions, has also been recognized as one of the reasons for the high morbidity of SARS viruses. [26−28] In fact, ACE2 is regarded as a favorable target of potential therapeutic agents counteracting SARS-CoV-2 infectivity, limiting its harmful effects. Consequently, high-resolution structures of the complex between the RBD and the extramembrane domain of ACE2 (RBD/ACE2) have been obtained. [22] The main patterns of interaction driving the formation of the RBD/ACE2 complex have also been pointed out and rationalized, highlighting the crucial differences with other coronaviruses. The hot spots assuring the efficient recognition by the RBD have been identified in the so-called peptide domain (PD) of the ACE2 receptor (Figure 1), consisting of an extended α-helical region, and traced back to the formation of a dense hydrogen bonding network with the RBD.
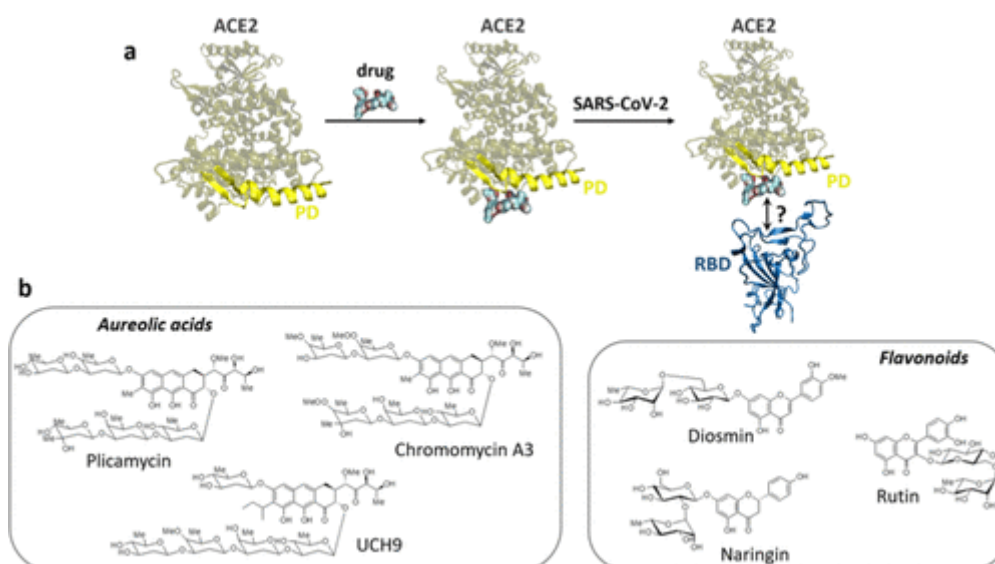
Figure 1. (a) Depiction of human angiotensin-converting enzyme 2 (ACE2) considering possible interactions of its peptide domain (PD) with administered drugs, which could in turn limit or prevent SARS-CoV-2 recognition through its active receptor binding domain (RBD). (b) Structures of the drugs being studied: aureolic acids, including plicamycin, chromomycin A3, and UCH9, and flavonoids, including diosmin, rutin, and naringin.

Different therapeutic strategies could be envisaged. On one hand, drugs could bind to the RBD, as is the case for small peptides (29−31) and neutralizing monoclonal antibodies. (32) Nevertheless, possible mutations of the RBD may decrease the efficiency of a treatment based on this approach. (33,34) On the other hand, an efficient therapeutic strategy could rely on the inhibition, by putative drugs, of the ACE2 PD to prevent the formation, or at least strongly destabilize, the RBD/ACE2 complex to reduce the virus infecting potential as schematized in Figure 1. ACE2 is known to act as a glycoprotein developing favorable interactions with sugar moieties, (35) which could also favorably compete with the RBD in establishing hydrogen bonds with the PD site.

In this work, we aim to provide a comprehensive analysis of the molecular bases allowing the favorable interaction between the SARS-CoV-2 RBD and the ACE2 receptor, hence allowing its easy entrance into the cell, by using extended all-atom molecular dynamics (MD) simulations. This will also include the calculation of the binding free energy for the formation of the protein complex, hence providing, for the first time, an assessment of the thermodynamics of SARS-CoV-2 recognition. Furthermore, the possible interaction of glycosylated potential therapeutic agents with ACE2 and their inhibition capacity over the PD will also be analyzed. Indeed, both spike and ACE2 proteins do have glycosylation sites but do not interfere with the ACE2/RBD interaction area, (22,36−38) and most probably are mainly related to protein folding and stabilization. (39)

To investigate the possible binding modes of the proposed drugs, a blind docking study considering the whole ACE2 geometry was performed using Autodock Vina software. (40) Prior to virtual screening, the three-dimensional geometry of each drug was built with Discovery Studio 2.1. The same program was used to add hydrogen atoms and assign bond orders, hybridization, and charges to ACE2, extracted from Protein Data Bank (PDB) entry 6M17. (22) The rotatable bonds of all drugs were allowed to rotate freely, as it was previously found to be a proper approach in SARS-CoV-2-related studies (41−43) and in other fields (44) (see the Supporting Information for details). For each drug, 50 independent calculations including the 20 lowest binding energies (1000 structures in total) were scrutinized for statistical analysis of the binding pockets and to select representative geometries to run the following molecular dynamics simulations.

The structure of the RBD/ACE2 complex was extracted from PDB entry 6M17, adding the previously selected drug geometry (from docking) and deleting the ACE2 C-terminal α-helix to diminish the computational expenses while not hampering the proper description of any ACE2 functional domain. In greater detail, the control simulation (i.e., the RBD/ACE2 complex without the drug) was run by taking the structure directly from the PDB. For the other simulations, including a drug at the RBD/ACE2 interface, the same PDB was initially considered. In some cases, the drug structure (taken from docking with ACE2) did not interfere with the complex, and therefore, MD equilibration was performed as for the control simulation; in other cases, the contact of the drug with the RBD surface was too close, hence requiring an initial minimal displacement of the RBD crystal structure toward the solvent before MD equilibration. In all cases, the initial ACE2/drug dispositions correspond to the most relevant docking poses (see Figure 2). After the solvation with water molecules to build a cubic box and addition of the corresponding K^+ counterions to achieve neutrality, this procedure resulted in the setup of 10 systems, including the RBD/ACE2 reference (without any drug) and three RBD/ACE2/drug starting structures, corresponding to different ACE2/drug binding pockets, for each of the three selected drugs. All of the 300 ns MD simulations reported herein were run using the NAMD (45) code at 300 K and 1 atm, with the Amber99SB force field (46−48) to describe the proteins and TIP3P (49) water molecules. The force field of each drug has been parametrized through the GAFF procedure. (50) VMD (51) was used for visualization, inspection, and analysis.
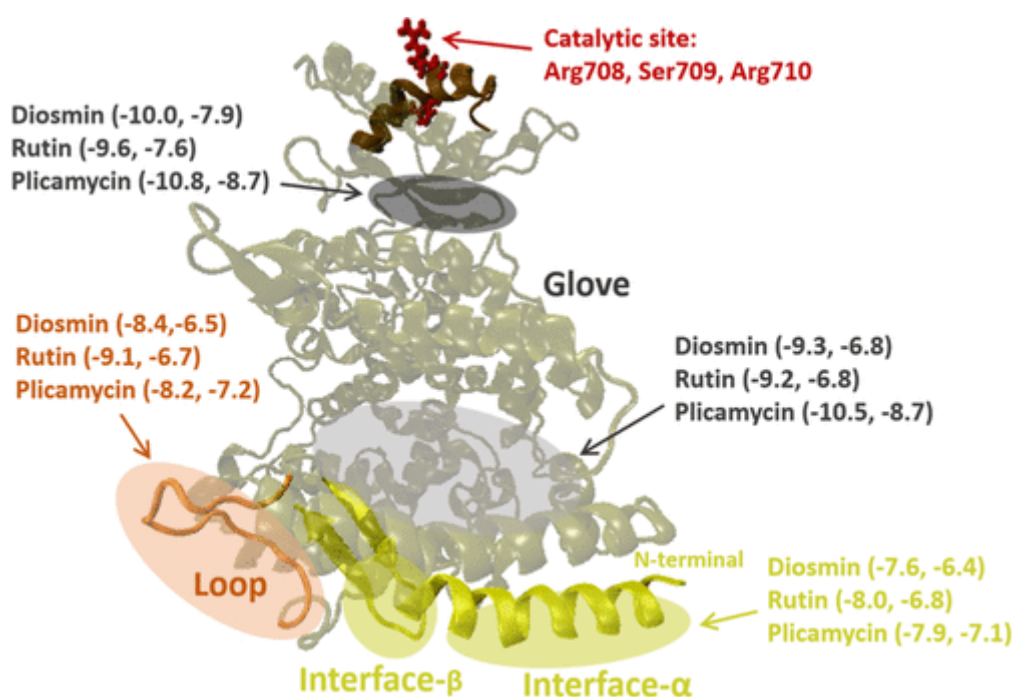
Figure 2. Different domains of ACE2: the peptide domain (PD) (yellow) formed by an N-terminal α-helix and a two-strand β-sheet, forming the potential interface region with the RBD; the loop at the side of the interface region (orange); and the glove domain bridging the interface region and the catalytic site (dark red), near the C-terminus. For each drug, the binding sites are shown together with the range of binding energy affinities in kilocalories per mole, which resulted from the docking study.

The potential of mean force (PMF) free energy profile was calculated by applying a recently developed combination of metadynamics (52) and adaptive biased force (eABF), (53) resulting in the meta-eABF (54,55) method implemented in the NAMD code. (45) As detailed below, it was applied, for the purpose of comparison, to the RBD/ACE2 reference and to the same system including plicamycin in the interface-β binding pocket, necessitating a 1 µs simulation to properly sample the defined distance between ACE2 and the RBD.

For the purpose of comparison, the ACE2/drug binding free energy was also estimated from the equilibrium MD simulations by applying the MM/GBSA methodology (i.e., molecular mechanics combined with the generalized Born surface area continuum solvation method), as implemented in the Amber interface. (56)

In particular, as illustrated in Figure 1b, we considered two classes of widely available compounds and already used in clinical applications: antibiotics based on aureolic acids (plicamycin, chromomycin A3, and UCH9) and flavonoids (diosmin, rutin, and naringin). This specific selection was guided, on one hand, by the medical necessity of proposing drugs that are available and already used in clinical applications, thus avoiding timely and economically expensive tests on eventually newly

designed drugs in the quest for COVID-19 solutions. On the other hand, from a chemical point of view, we looked for glycosylated potential drugs, being sensitive to ACE2, to produce interactions with glycans. Moreover, because the ACE2/RBD interaction is mainly driven by hydrogen bonds and other polar interactions, (20) we looked for structures maximizing the number of -OH and -C꞊O groups. At the same time, the presence of aromatic polycycles (where such groups are anchored) is usually considered to be beneficial for interacting with biological membranes, because these aromatic polycycles are essential for the drug to bind to the target. (57,58)

Our multiscale methods include the use of molecular docking studies to assess the presence of suitable binding poses leading to possible PD inhibition, extended MD simulations to assess the effects of the binding of the drug on the stability and dynamics of the RBD/ACE2 complex, and the use of free energy methods to unravel the effects of the drug in destabilizing the RBD/ACE2 complex as compared to the native situation.

The results of the flexible drug docking are reported in Figure 2 and more extensively in Figure S1. All of the chosen compounds are previewed to form stable aggregates with ACE2, although slight differences in the binding energies are evidenced. Importantly, four main interaction hot spots are identified encompassing different regions of the enzyme (Figure 2). The results of the docking indicate that the four regions are generally competitive for all of the compounds being studied. Three of them are significant in terms of RBD/ACE2 inhibition, whereas only one site is clearly out of reach of the RBD interaction area and is instead situated close to the ACE2 catalytic region (21) (Figure 2, dark gray). For obvious structural reasons, this interacting site is most unlikely to significantly perturb the binding with the RBD and hence is not considered in the following.

On the other hand, the three residual interacting sites lie close to the RBD binding region. The glove site (light gray in Figure 2) constitutes a slightly buried pocket formed by ACE2 α-helices positioned just on top of the PD. The loop domain (orange in Figure 2) consists mainly of an unstructured loop lying close to the RBD upon the formation of the complex. Finally, two sites are identified directly positioned on the N-terminal PD area (yellow in Figure 2) and named interface-α and interface-β. Interestingly, while interface-α can be observed for all of the docked compounds, interface-β is mainly occupied by aureolic acids and plicamycin in particular. Obviously, these latter sites clearly represent the most promising candidates for ACE2 inhibition because they are susceptible to strong perturbation of the recognition and binding of the RBD. Finally, it is important to point out that no specific interaction with the ACE2 catalytic

active site, composed of the amino acid triad of Arg708, Ser709, and Arg710, (21) has been observed. This fact is extremely important because, while blocking formation of the RBD/ACE2 complex is supposed to be the most beneficial, the inhibition of the native catalytic activity of the enzyme should be avoided to limit the possible side effects of the drug.

The free energy of binding between the ACE2/RBD complex and the different drugs has also been obtained by applying the MM/GBSA methodology, confirming the global tendency sketched out by the docking results, i.e., the stable interaction between ACE2 and the potential drugs (Figure S8). Note that plicamycin appears as the most favorable binder but also shows the larger standard deviation when placed at interface-α. This is due to the partial destabilization of the ACE2/RBD complex as it will be detailed in the following.

On the basis of the docking results, and to provide a reasonable sampling and description of the effects produced by the different modes, we have chosen three compounds to perform equilibrium MD simulations of the ACE2/RBD complex in the presence of the drug, namely diosmin, rutin, and plicamycin. For each of these compounds, three independent MD trajectories have been obtained, starting from initial conditions corresponding to different binding poses: glove and loop sites, interface-α, and interface-β. MD of the native RBD/ACE2 complex in the absence of any ligand was also performed for comparison. In all cases, equilibrium MD yielded stable and persistent aggregates between the RBD/ACE2 complex and the drugs, as evidenced by the value of the root-mean-square deviation (RMSD) reported in Figure S6, and by the fact that neither the macroscopic disruption of the RBD/ACE2 complex nor the ejection of the drug was observed. However, important differences can be observed depending on the individual drugs and on the specific interaction site, as illustrated in Figure 3.
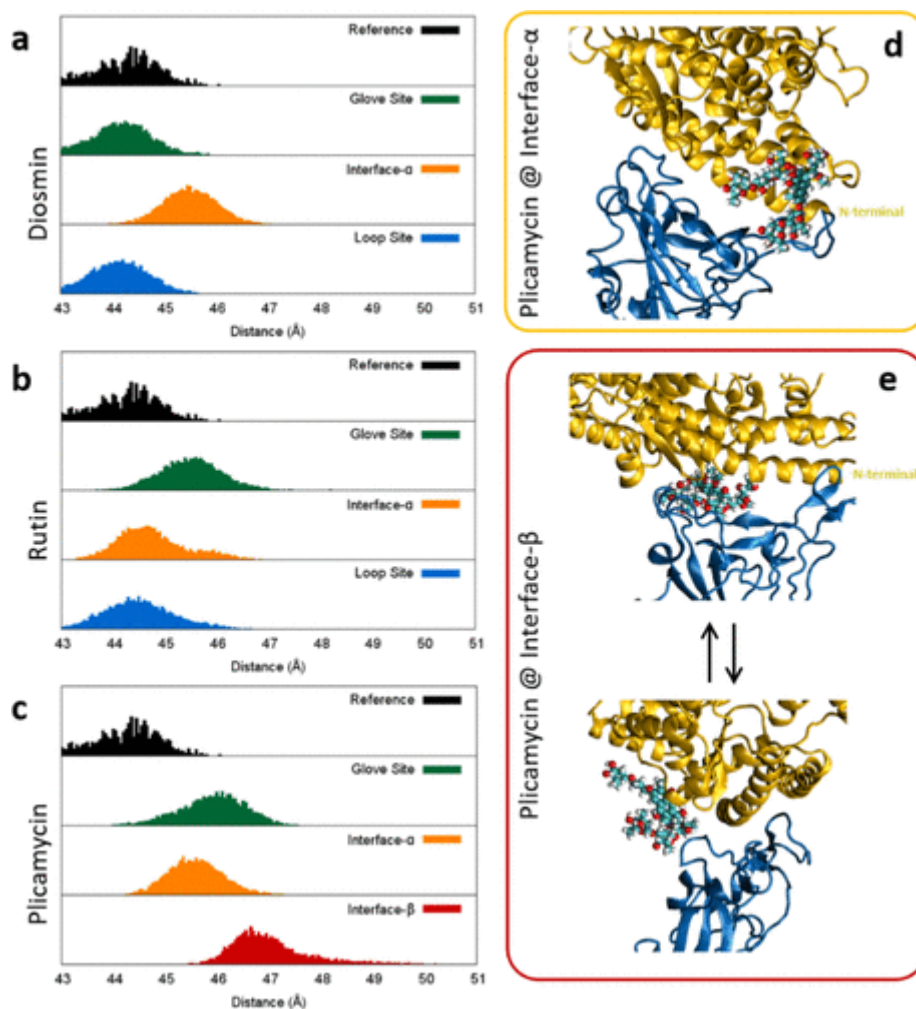
Figure 3. Distribution function of the RBD/ACE2–PD distance in the presence of (a) diosmin, (b) rutin, and (c) plicamycin at the different binding modes. The results for the RBD/ACE2 complex in the absence of any drug (reference) are also shown for comparison. (d) Representative snapshot of plicamycin at interface-α. (e) Representative snapshots of the two plicamycin conformations in equilibrium at interface-β.

A most useful indicator for quantifying the effects of the drug on the RBD/ACE2 complex is the distribution of the distance between their centers of mass at the interface area (see the Supporting Information for the full definition and Figure S2 for the corresponding time series), because this distance increases when the protein−protein interactions are weakened. Representative snapshots extracted from the different MD trajectories are also provided in panels d and e of Figure 3 and Figure S5, giving a pictorial view of the induced destabilization. In the case of diosmin (Figure 3a), both loop and glove sites have no noticeable effect in destabilizing the complex, while the maximum of the distribution is even slightly shifted to shorter distances compared to the reference. As expected, due to the better exposition to the PD area, the interface-α interaction mode, instead, presents a slight increase of ~2 Å in the

distribution maximum. However, the global efficiency of diosmin as a valuable ACE2 inhibitor appears to be quite limited.

Conversely, rutin (Figure 3b) shows clearly improved properties as identified by the fact that all three interaction modes (loop, glove, and interface-α) induce a considerable increase in the distance between the centers of mass and hence are indicative of the weakening of the protein−protein interactions. Interestingly, the distribution for the interface-α presents a secondary maximum at a larger distance, which points to the emergence of a conformational equilibrium and hence an even more evident destabilization. Thus, this fact also confirms the peculiar role played by interface-α binders as opposed to the other sites.

Finally, plicamycin (Figure 3c) definitively appears as the most promising compound. In fact, it presents a novel interaction mode, interface-β, that is directly facing the RBD interaction area, and that can also be achieved by the sliding of the ligand from the less efficient and spatially close loop site. All of the interaction modes are correlated to a noticeable increase in the protein−protein distance. As far as the novel interface-β mode is concerned, we observe not only a larger shift in the distribution maximum (>3 Å) but also and especially the emergence of a strong asymmetry in the distribution with a tail extending noticeably in the longer distance region (>5 Å from the reference). The effects of plicamycin on the RBD/ACE2 complex can also be appreciated by the analysis of representative snapshots for interface-α (Figure 3d), which clearly show the positioning of the drug at the interface between the two proteins, and for interface-β (Figure 3e), in which the presence of an even more open form already visualizes a partial disruption of the RBD/ACE2 complex (see also the Supporting Information video).

To better understand those global effects, we also perform a detailed analysis of the specific RBD/ACE2 interactions that are perturbed by the presence of the drugs, in particular the favorable polar interactions that ensure protein/protein binding. The equilibrium MD of the native RBD/ACE2 complex has allowed us to confirm the amino acids interacting between the two proteins, as shown in Figure 4. Unsurprisingly, the most important amino acids assuring the interactions are placed at interface-α and -β and are mostly acting through hydrogen bonding, as confirmed by different independent studies. (15,22) Panels a−c of Figure 4 report the difference in the average number of hydrogen bonds per ACE2 amino acid in the presence or absence of the drug. Globally, these parameters confirm the tendency already evidenced in Figure 3, and indeed, diosmin, especially in glove and loop sites, is producing a less important perturbation compared to the other ligands, even increasing the strength of the hydrogen bonds mediated by Glu37

(glove) and Asp38 (loop) while the number of hydrogen bonds weakened by diosmin at the interface-α, and especially in the N-terminal region of the PD, is clearly more important (see Table S1 for more details). The behavior of rutin is similar; however, the weakening of interactions takes place mainly in the N-terminal area (see Table S2 for more details). In contrast, once again, a different behavior is observed for plicamycin, especially at interface-β. In this case, hydrogen bonds encompassing the whole PD region are significantly weakened. In particular, for this specific binding site, one should point out the almost total disruption of the Asp355···Thr500 and Lys353···Gly502 hydrogen bonds, although in this latter case the strong interaction with Gly502 is replaced by several weak hydrogen bonds with other amino acids (see Table S3). In addition, we observe that the drug also weakens indirect hydrogen bonds, i.e., formed through a bridging water molecule, albeit to a lower extent with respect to direct hydrogen bonds (see Figure S3). It should be remarked that, independent of the binding site, the drug interacts mainly with ACE2 and not with the RBD, through different types of noncovalent interactions as evidenced in Figure S4. This confirms our strategy based on blocking solely the domain of ACE2 susceptible to RBD recognition.
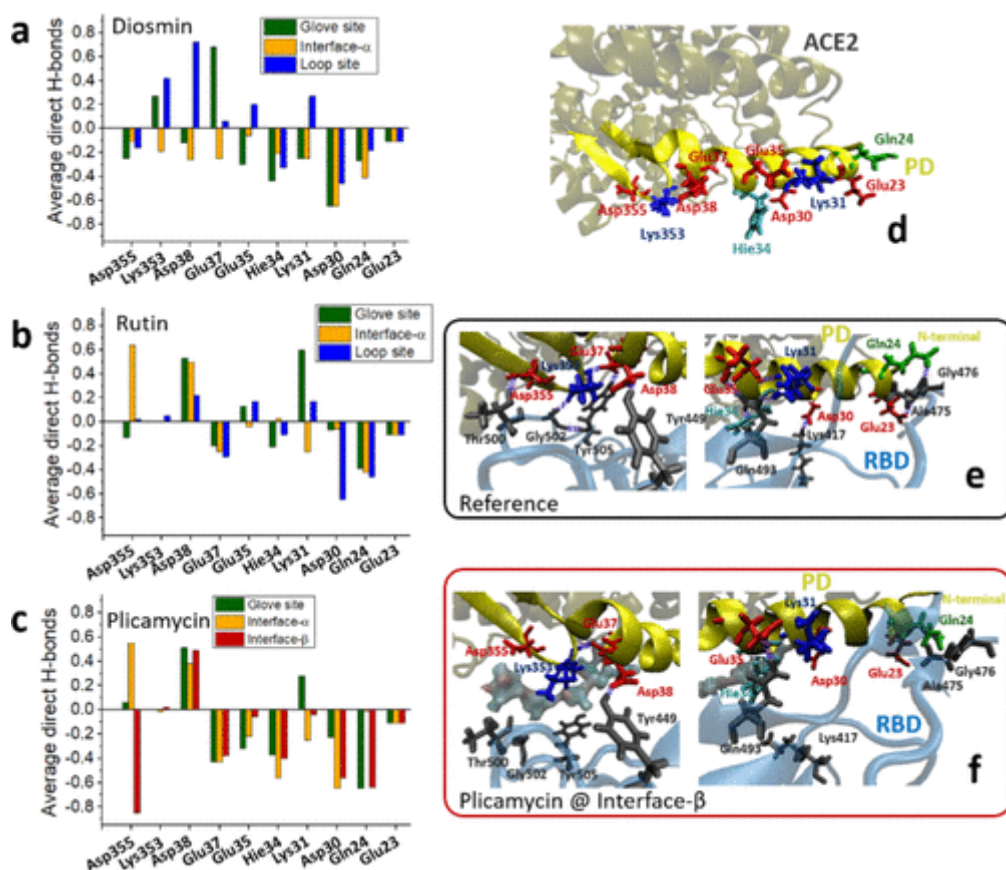

Figure 4. Histogram showing the increase (positive values) or decrease (negative values) in the number of direct H-bonds between ACE2-(PD) and the RBD for (a) diosmin, (b) rutin, and (c) plicamycin, averaged along each trajectory. (d) ACE2 (PD) amino acids involved in the formation of direct H-bonds. Color code: red for negatively

charged, blue for positively charged, green for polar, and cyan for neutral His ε-protonated. (e) H-Bonding network at the interface-β (left) and interface-α (right) sites of the untreated ACE2-(PD)/RBD reference system. RBD amino acid side chains are colored gray. (f) Same as panel e, but including plicamycin (visualized in surface representation) interacting at interface-β.

The fact that plicamycin is effectively acting over all of the ACE2/RBD interaction region is essential in explaining the strong destabilization of the protein/protein complex. This can be observed in panels e and f of Figure 4, in which we report the comparison of a representative snapshot showing the hydrogen bond network for the reference complex and plicamycin at interface-β. The breaking of the interactions in both contact regions is evident and is certainly related to the strong destabilization of the complex yielding an open conformation characterized by a much larger protein/protein distance.

The results presented offer a coherent, yet still qualitative, scenario. To better quantify the effect of the best candidate, i.e., plicamycin at interface-β, we determine the thermodynamic properties of the RBD/ACE2 complex. To do so, we calculate the free energy profile along the distance between the center of mass of the two proteins, in the presence and absence of plicamycin (Figure 5). The free energy profile for the native complex is characterized by a rather deep energy well accounting for a binding free energy of ~3.0 kcal/mol at a distance of 70 Å. We note that, due to the application of harmonic walls in the e-ABF procedure and the inclusion of some rotational constraints, the calculated difference in stability induced by the presence of the drug should be considered from a relative, rather than absolute, point of view. As expected, no energetic barrier is evidenced for the formation of the complex, at least considering the RBD in its active conformation, confirming the high affinity of the RBD for ACE2. Upon addition of plicamycin, we first note, consistent with the equilibrium MD, an increase in the distance between the centers of mass corresponding to the minimum free energy. More importantly, the free energy profile becomes distinctly shallower and the binding energy decreases to ~2.1 kcal/mol at a distance of 70 Å, hence indicating a clear destabilization of the RDB/ACE2 complex. Interestingly, a secondary, less stable minimum at a shorter distance is also evidenced, justifying, together with the shallow free energy profile, the two conformations observed by equilibrium MD and the detection of a semidissociated conformation.
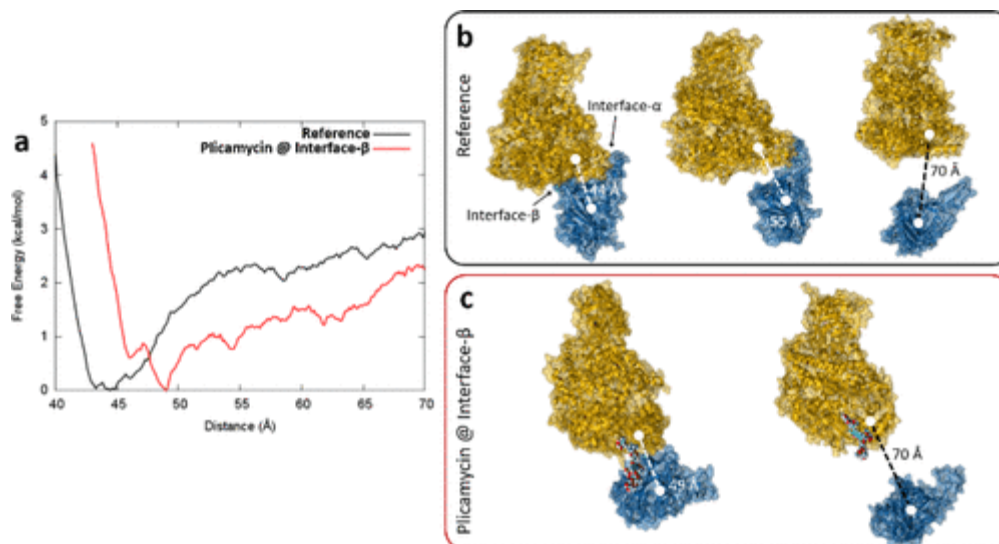
Figure 5. (a) Free energy profiles of the RBD/ACE2 complex in the absence and presence of plicamycin at interface-β. (b) Snapshots of the reference system at its free energy minimum, when detaching at interface-β, and when completely separated. (c) Snapshots of the complex in the presence of plicamycin at interface-β, at its free energy minimum and separated.

In summary, the very favorable and strong interaction between the SARS-CoV-2 spike protein, through its active RBD, and ACE2 represents a peculiarity of this coronavirus that should be correlated to its extremely high transmissibility rate, and hence to its dangerousness, even as compared to the previous SARS-CoV. (17) By using extended equilibrium MD, we have confirmed that this affinity is mostly due to the presence of an extended network of favorable hydrogen bonds, encompassing the rather spread N-terminal PD of ACE2, as coherently confirmed by our results and other independent studies. (15,16,20,59) In addition, we also provide the first estimation of the binding free energy of the RBD/ACE2 complex that also points to very strong and favorable interactions.

Understanding the molecular mechanism at the base of the strong interaction between ACE2 and RBD is crucial to rationalizing the function and behavior of SARS-CoV-2, because the former constitutes the entry point of the virus in human cells. As a consequence, its inhibition and the further weakening of the formation of the RBD/ACE2 complex represent a possible therapeutic strategy to be pursued. Suitable ligands for performing such a task should form strong and specific interactions with the PD region, while they should not interact with the catalytic domain of ACE2 to avoid serious secondary effects. As shown by molecular docking, we propose an ensemble of glycosylated drugs, already available, that present different modes of interaction with ACE2. MD simulations have clearly shown that while almost all of the chosen compounds have non-negligible effects in weakening the RBD/ACE2 interaction, as witnessed by the wide distribution of the distance between

the centers of mass of the proteins and by the analysis of the hydrogen bonding network, their efficiency may vary considerably. In particular, the aureolic acid plicamycin clearly stands out as the lead compound. Its efficacy is due to its capacity to perturb almost all of the PD region of ACE2, considerably disrupting the hydrogen bonding network at both interfaces (α and β). Such an efficiency is already evident at the equilibrium MD by the appearance of partially dissociated conformations presenting a larger protein/protein distance, the interaction through almost all of the PD being broken. This qualitative behavior is also confirmed by the binding free energy profile that, when compared with that of the native complex, yields an increased protein/protein distance corresponding to the minimum free energy, while the complexation free energy is reduced by ~30%. Our PMF for the native ACE2/RBD complex has also shown that unbinding preferably starts from the detachment of interface-β, further suggesting the suitability of plicamycin (Figure 5b,c) that is occupying this binding mode.

Hence, our results suggest that the antibiotic plicamycin, also known as mithramycin, could be a promising agent for preventing viral infection and hence reducing the virulence and morbidity of the SARS-CoV-2 pathogen. Tests of plicamycin, being already commercially and clinically approved, (60) to confirm its efficacy should be considered as a top priority, to be performed in vitro and in vivo. This should also include the assessment of its side effects such as hepatotoxicity, (61) which despite usually being transient and asymptomatic could limit its therapeutic use in certain patients with limited hepatic function. This is especially relevant in the context of emergency and urgency caused by the 2020 COVID-19 pandemic outbreak. In addition, we mention that related aureolic acid compounds such as durhamycin A (62) and chromomycin (63) have already shown antiviral activity against HIV.

In addition to specifically pinpointed plicamycin, we also established on a firm basis the interactions between the RBD and ACE2, evidencing the most important amino acids that should be targeted to achieve an efficient weakening of the formation of the RBD/ACE2 complex. Such knowledge improves our understanding of the molecular bases leading to SARS-CoV-2 viral infection and can be efficiently used, in the long term, for rational molecular design procedures to enhance the efficacy of novel or existing drugs and to contrast possible mutations that could lead to resistant viral strains.

From a more methodological point of view, we also developed and optimized an efficient multiscale computational protocol, going from molecular docking to enhanced sampling and free energy techniques, that allows us to assess and quantify the fundamental interactions

between viral and human proteins and the effects of potential ligands in counteracting complex formation.

In the future, we plan to further analyze the RBD, and more generally SARS-CoV-2 spike structural and dynamical properties, as well as the possible alteration induced by possible ligands. In this context, the conformational equilibrium between the closed and open forms of RBD could be particularly attractive. The possible synergic effects of different ligands occupying distinct binding domains will also be taken into account in the computational protocol developed with this study.

Supporting Information

The Supporting Information is available free of charge at https://pubs.acs.org/doi/10.1021/acs.jpclett.0c02203. Extended computational details, results of the molecular docking for all of the compounds, analysis of the hydrogen bond patterns, time series of the distances between the centers of mass, indirect hydrogen bonds between the drugs and the solvent, additional representative snapshots, root-mean-square deviation values, and distribution function of the distance between ACE2-(PD) and each selected drug (Figures S1−S8, Tables S1−S3, and references) (PDF) Video showing the partial disruption of the RBD/ACE2 complex (MPG).

REFERENCES

(1) Watkins, J. Preventing a Covid-19 Pandemic. BMJ [Br. Med. J.] 2020, 368, m810. (2) Tang, B.; Wang, X.; Li, Q.; Bragazzi, N. L.; Tang, S.; Xiao, Y.; Wu, J. Estimation of the Transmission Risk of the 2019-NCoV and Its Implication for Public Health Interventions. J. Clin. Med. 2020, 9 (2), 462. (3) Cao, Z.; Zhang, Q.; Lu, X.; Pfeiffer, D.; Jia, Z.; Song, H.; Zeng, D. D. Estimating the Effective Reproduction Number of the 2019- NCoV in China. medRxiv 2020, DOI: 10.1101/2020.01.27.20018952. (4) Bedford, J.; Enria, D.; Giesecke, J.; Heymann, D. L.; Ihekweazu, C.; Kobinger, G.; Lane, H. C.; Memish, Z.; Oh, M.-d.; Sall, A.

A.; et al. COVID-19: Towards Controlling of a Pandemic. Lancet 2020, 395 (10229), 1015–1018. (5) Shi, H.; Han, X.; Jiang, N.; Cao, Y.; Alwalid, O.; Gu, J.; Fan, Y.; Zheng, C. Radiological Findings from 81 Patients with COVID-19 Pneumonia in Wuhan, China: A Descriptive Study. Lancet Infect. Dis. 2020, 20, 425. (6) Lai, C. C.; Shih, T. P.; Ko, W. C.; Tang, H. J.; Hsueh, P. R. Severe Acute Respiratory Syndrome Coronavirus 2 (SARS-CoV-2) and Coronavirus Disease-2019 (COVID-19): The Epidemic and the Challenges. Int. J. Antimicrob. Agents 2020, 55 (3), 105924. (7) Kooraki, S.; Hosseiny, M.; Myers, L.; Gholamrezanezhad, A. Coronavirus (COVID-19) Outbreak: What the Department of Radiology Should Know. J. Am. Coll. Radiol. 2020, 17 (4), 447–451. (8) Liu, Y.; Gayle, A. A.; Wilder-Smith, A.; Rocklöv, J. The Reproductive Number of COVID-19 Is Higher Compared to SARS Coronavirus. J. Travel Med. 2020, 27 (2), taaa021. (9) Yuen, K. S.; Ye, Z. W.; Fung, S. Y.; Chan, C. P.; Jin, D. Y. SARSCoV-2 and COVID-19: The Most Important Research Questions. Cell Biosci. 2020, 10 (1), 1–5. (10) Wilder-Smith, A.; Chiew, C. J.; Lee, V. J. Can We Contain the COVID-19 Outbreak with the Same Measures as for SARS? Lancet Infect. Dis. 2020, 20 (5), e102–e110. (11) Dong, E.; Du, H.; Gardner, L. An Interactive Web-Based Dashboard to Track COVID-19 in Real Time. Lancet Infect. Dis. 2020, 20 (5), 533–534. (12) Andersen, K. G.; Rambaut, A.; Lipkin, W. I.; Holmes, E. C.; Garry, R. F. The Proximal Origin of SARS-CoV-2. Nat. Med. 2020, 26 (4), 450–452. (13) Tang, X.; Wu, C.; Li, X.; Song, Y.; Yao, X.; Wu, X.; Duan, Y.; Zhang, H.; Wang, Y.; Qian, Z.; et al. On the Origin and Continuing Evolution of SARS-CoV-2. Natl. Sci. Rev. 2020, 7 (6), 1012–1023. (14) Wang, Q.; Zhang, Y.; Wu, L.; Niu, S.; Song, C.; Zhang, Z.; Lu, G.; Qiao, C.; Hu, Y.; Yuen, K.-Y.; et al. Structural and Functional Basis of SARS-CoV-2 Entry by Using Human ACE2. Cell 2020, 181 (4), 894–904.e9. (15) Shang, J.; Ye, G.; Shi, K.; Wan, Y.; Luo, C.; Aihara, H.; Geng, Q.; Auerbach, A.; Li, F. Structural Basis of Receptor Recognition by SARS-CoV-2. Nature 2020, 581 (7807), 221–224. (16) Lan, J.; Ge, J.; Yu, J.; Shan, S.; Zhou, H.; Fan, S.; Zhang, Q.; Shi, X.; Wang, Q.; Zhang, L.; et al. Structure of the SARS-CoV-2 Spike Receptor-Binding Domain Bound to the ACE2 Receptor. Nature 2020, 581 (7807), 215–220. (17) Wrapp, D.; Wang, N.; Corbett, K. S.; Goldsmith, J. A.; Hsieh, C. L.; Abiona, O.; Graham, B. S.; McLellan, J. S. Cryo-EM Structure of the 2019-NCoV Spike in the Prefusion Conformation. Science 2020, 367 (6483), 1260–1263. (18) Chen, H.; Du, Q. Potential Natural Compounds for Preventing SARS-CoV-2 (2019-NCoV) Infection. Preprints 2020, DOI: 10.20944/preprints202001.0358.v3. (19) Hognon, C.; Miclot, T.; Garcia-Iriepa, C.; Frances-Monerris, A.; Grandemange, S.; Terenzi, A.; Marazzi, M.; Barone, G.; Monari, A. Role of RNA Guanine Quadruplexes in Favoring the Dimerization of SARS Unique Domain in Coronaviruses. J. Phys. Chem. Lett. 2020, 11, 5661. (20) Spinello, A.; Saltalamacchia, A.; Magistrato, A. Is the Rigidity of SARS-CoV-2 Spike Receptor-Binding Motif the Hallmark for Its Enhanced Infectivity? Insights from All-Atom Simulations. J. Phys. Chem. Lett. 2020, 11, 4785–4790. (21) Lai, Z. W.; Hanchapola, I.; Steer, D. L.; Smith, A. I. Angiotensin-Converting Enzyme 2 Ectodomain Shedding CleavageSite Identification: Determinants and Constraints. Biochemistry 2011, 50 (23), 5182–5194. (22) Yan, R.; Zhang, Y.; Li, Y.; Xia, L.; Guo, Y.; Zhou, Q. Structural Basis for the Recognition of SARS-CoV-2 by Full-Length Human ACE2. Science 2020, 367 (6485), 1444–1448. (23) Oudit, G. Y.; Crackower, M. A.; Backx, P. H.; Penninger, J. M. The Role of ACE2 in Cardiovascular Physiology. Trends Cardiovasc. Med. 2003, 13 (3), 93–101. (24) Crackower, M. A.; Sarao, R.; Oudit, G. Y.; Yagil, C.; Kozieradzki, I.; Scanga, S. E.; Oliveira-dos-Santos, A. J.; da Costa, J.; Zhang, L.; Pei, Y.; Scholey, J.; Ferrario, C. M.; Manoukian, A. S.; Chappell, M. C.; Backx, P. H.; Yagil, Y.; Penninger, J. M. AngiotensinConverting Enzyme 2 Is an Essential Regulator of Heart Function. Nature 2002, 417, 822–828. (25) Böhmer, C.; Sopjani, M.; Klaus, F.; Lindner, R.;

Laufer, J.; Jeyaraj, S.; Lang, F.; Palmada, M. The Serum and Glucocorticoid Inducible Kinases SGK1−3 Stimulate the Neutral Amino Acid Transporter SLC6A19. Cell. Physiol. Biochem. 2010, 25 (6), 723−732. (26) Verity, R.; Okell, L. C.; Dorigatti, I.; Winskill, P.; Whittaker, C.; Imai, N.; Cuomo-Dannenburg, G.; Thompson, H.; Walker, P. G. T.; Fu, H.; et al. Estimates of the Severity of Coronavirus Disease 2019: A Model-Based Analysis. Lancet Infect. Dis. 2020, 20 (6), 669−677. (27) Vincent, J.-L.; Taccone, F. S. Understanding Pathways to Death in Patients with COVID-19. Lancet Respir. Med. 2020, 8 (5), 430− 432. (28) Yuan, J.; Li, M.; Lv, G.; Lu, Z. K. Monitoring Transmissibility and Mortality of COVID-19 in Europe. Int. J. Infect. Dis. 2020, 95, 311−315. (29) Whisenant, J.; Burgess, K. Blocking Coronavirus 19 Infection via the SARS-CoV-2 Spike Protein: Initial Steps. ACS Med. Chem. Lett. 2020, 11 (6), 1076−1078. (30) Qiao, B.; Olvera de la Cruz, M. Enhanced Binding of SARSCoV-2 Spike Protein to Receptor by Distal Polybasic Cleavage Sites. ACS Nano 2020, 14 (8), 10616−10623. (31) Han, Y.; Kral, P. Computational Design of ACE2-Based Peptide Inhibitors of SARS-CoV-2. ACS Nano 2020, 14 (4), 5143− 5147. (32) Ju, B.; Zhang, Q.; Ge, J.; Wang, R.; Sun, J.; Ge, X.; Yu, J.; Shan, S.; Zhou, B.; Song, S.; et al. Human Neutralizing Antibodies Elicited by SARS-CoV-2 Infection. Nature 2020, 584, 115−119. (33) Jia, Y.; Shen, G.; Zhang, Y.; Huang, K.-S.; Ho, H.-Y.; Hor, W.- S.; Yang, C.-H.; Li, C.; Wang, W.-L. Analysis of the Mutation Dynamics of SARS-CoV-2 Reveals the Spread History and Emergence of RBD Mutant with Lower ACE2 Binding Affinity. bioRxiv 2020, DOI: 10.1101/2020.04.09.034942. (34) Ou, J.; Zhou, Z.; Dai, R.; Zhang, J.; Lan, W.; Zhao, S.; Wu, J.; Seto, D.; Cui, L.; Zhang, G.; et al. Emergence of RBD Mutations in Circulating SARS-CoV-2 Strains Enhancing the Structural Stability and Human ACE2 Receptor Affinity of the Spike Protein. bioRxiv 2020, DOI: 10.1101/2020.03.15.991. (35) Prabakaran, P.; Xiao, X.; Dimitrov, D. S. A Model of the ACE2 Structure and Function as a SARS-CoV Receptor. Biochem. Biophys. Res. Commun. 2004, 314 (1), 235−241. (36) Chen, Y.; Guo, Y.; Pan, Y.; Zhao, Z. J. Structure Analysis of the Receptor Binding of 2019-NCoV. Biochem. Biophys. Res. Commun. 2020, 525 (1), 135−140. (37) Li, F.; Li, W.; Farzan, M.; Harrison, S. C. Structural Biology: Structure of SARS Coronavirus Spike Receptor-Binding Domain Complexed with Receptor. Science 2005, 309 (5742), 1864−1868. (38) Chakraborti, S.; Prabakaran, P.; Xiao, X.; Dimitrov, D. S. The SARS Coronavirus S Glycoprotein Receptor Binding Domain: Fine Mapping and Functional Characterization. Virol. J. 2005, 2 (1), 73. (39) ACS. Adding the Missing Sugars to Coronavirus Protein Structures. Chem. Eng. News 2020, 98 (16), 24−25. (40) Trott, O.; Olson, A. J. AutoDock Vina: Improving the Speed and Accuracy of Docking with a New Scoring Function, Efficient Optimization, and Multithreading. J. Comput. Chem. 2009, 31 (2), 455−461. (41) Villas-Boas, G. R.; Rescia, V. C.; Paes, M. M.; Lavorato, S. N.; Magalhaes-Filho, M. F. de; Cunha, M. S.; Simo ̃es, R. da C.; Lacerda, R. B. de; Freitas-Junior, R. S. de; Ramos, B. H. da S.; et al. No TitThe New Coronavirus (SARS-CoV-2): A Comprehensive Review on Immunity and the Application of Bioinformatics and Molecular Modeling to the Discovery of Potential Anti-SARS-CoV-2 Agents. Molecules 2020, 25 (18), 4086. (42) Gentile, D.; Patamia, V.; Scala, A.; Sciortino, M. T.; Piperno, A.; Rescifina, A. Putative Inhibitors of SARS-COV-2 Main Protease from a Library of Marine Natural Products: A Virtual Screening and Molecular Modeling Study. Mar. Drugs 2020, 18 (4), 225. (43) Huynh, T.; Wang, H.; Luan, B. In Silico Exploration of Molecular Mechanism of Clinically Oriented Drugs for Possibly Inhibiting SARS-CoV-2's Main Protease. J. Phys. Chem. Lett. 2020, 11 (11), 4413−4420. (44) Pachon-Angona, I.; Refouvelet, B.; Andry ́s, R.; Martin, H.; Luzet, V.; Iriepa, I.; Moraleda, I.; Diez-Iriepa, D.; Oset-Gasque, M. J.; Marco-Contelles, J.; et al. Donepezil + Chromone + Melatonin Hybrids as Promising Agents for Alzheimer's Disease Therapy. J. Enzyme Inhib. Med. Chem. 2019,

34 (1), 479–489. (45) Phillips, J. C.; Braun, R.; Wang, W.; Gumbart, J.; Tajkhorshid, E.; Villa, E.; Chipot, C.; Skeel, R. D.; Kale, L.; Schulten, K. Scalable Molecular Dynamics with NAMD. J. Comput. Chem. 2005, 26 (16), 1781–1802. (46) Maier, J. A.; Martinez, C.; Kasavajhala, K.; Wickstrom, L.; Hauser, K. E.; Simmerling, C. Ff14SB: Improving the Accuracy of Protein Side Chain and Backbone Parameters from Ff99SB. J. Chem. Theory Comput. 2015, 11 (8), 3696–3713. (47) Galindo-Murillo, R.; Robertson, J. C.; Zgarbova, M.; S ̌poner, J.; Otyepka, M.; Jurecka, P.; Cheatham, T. E. Assessing the Current State ̌of Amber Force Field Modifications for DNA. J. Chem. Theory Comput. 2016, 12 (8), 4114–4127. (48) Zgarbova, M.; S ̌poner, J.; Otyepka, M.; Cheatham, T. E.; Galindo-Murillo, R.; Jurecka, P. Refinement of the Sugar-Phosphate ̌Backbone Torsion Beta for AMBER Force Fields Improves the Description of Z- and B-DNA. J. Chem. Theory Comput. 2015, 11 (12), 5723–5736. (49) Jorgensen, W. L.; Chandrasekhar, J.; Madura, J. D.; Impey, R. W.; Klein, M. L. Comparison of Simple Potential Functions for Simulating Liquid Water. J. Chem. Phys. 1983, 79 (2), 926–935. (50) Wang, J.; Wolf, R. M.; Caldwell, J. W.; Kollman, P. A.; Case, D. A. Development and Testing of a General Amber Force Field. J. Comput. Chem. 2004, 25 (9), 1157–1174. (51) Humphrey, W.; Dalke, A.; Schulten, K. VMD: Visual Molecular Dynamics. J. Mol. Graphics 1996, 14 (1), 33–38. (52) Barducci, A.; Bonomi, M.; Parrinello, M. Metadynamics. Wiley Interdiscip. Rev.: Comput. Mol. Sci. 2011, 1 (5), 826–843. (53) Zhao, T.; Fu, H.; Lelievre, T.; Shao, X.; Chipot, C.; Cai, W. The Extended Generalized Adaptive Biasing Force Algorithm for Multidimensional Free-Energy Calculations. J. Chem. Theory Comput. 2017, 13 (4), 1566–1576. (54) Fu, H.; Zhang, H.; Chen, H.; Shao, X.; Chipot, C.; Cai, W. Zooming across the Free-Energy Landscape: Shaving Barriers, and Flooding Valleys. J. Phys. Chem. Lett. 2018, 9 (16), 4738–4745. (55) Fu, H.; Shao, X.; Cai, W.; Chipot, C. Taming Rugged Free Energy Landscapes Using an Average Force. Acc. Chem. Res. 2019, 52 (11), 3254–3264. (56) Miller, B. R .; McGee, T. D.; Swails, J. M.; Homeyer, N.; Gohlke, H.; Roitberg, A. E. MMPBSA.Py: An Efficient Program for End-State Free Energy Calculations. J. Chem. Theory Comput. 2012, 8 (9), 3314–3321. (57) Gattuso, H.; Marazzi, M.; Dehez, F.; Monari, A. Deciphering the Photosensitization Mechanisms of Hypericin towards Biological Membranes. Phys. Chem. Chem. Phys. 2017, 19 (34), 23187–2319. (58) Marazzi, M.; Gattuso, H.; Giussani, A.; Zhang, H.; NavarreteMiguel, M.; Chipot, C.; Cai, W.; Roca-Sanjuan, D.; Dehez, F.; Monari, A. Induced Night Vision by Singlet-Oxygen-Mediated Activation of Rhodopsin. J. Phys. Chem. Lett. 2019, 10 (22), 7133– 7140. (59) Lupala, C. S.; Li, X.; Lei, J.; Chen, H.; Qi, J.; Liu, H.; Su, X. Computational Simulations Reveal the Binding Dynamics between Human ACE2 and the Receptor Binding Domain of SARS-CoV-2 Spike Protein. bioRxiv 2020, DOI: 10.1101/2020.03.24.005561. (60) Taylor, D. J.; Parsons, C. E.; Han, H.; Jayaraman, A.; Rege, K. Parallel Screening of FDA-Approved Antineoplastic Drugs for Identifying Sensitizers of TRAIL-Induced Apoptosis in Cancer Cells. BMC Cancer 2011, 11 (1), 470. (61) Sissung, T. M.; Huang, P. A.; Hauke, R. J.; McCrea, E. M.; Peer, C. J.; Barbier, R. H.; Strope, J. D.; Ley, A. M.; Zhang, M.; Hong, J. A.; et al. Severe Hepatotoxicity of Mithramycin Therapy Caused by Altered Expression of Hepatocellular Bile Transporters. Mol. Pharmacol. 2019, 96 (2), 158–167. (62) Jayasuriya, H.; Lingham, R. B.; Graham, P.; Quamina, D.; Herranz, L.; Genilloud, O.; Gagliardi, M.; Danzeisen, R.; Tomassini, J. E.; Zink, D. L.; et al. Durhamycin A, a Potent Inhibitor of HIV Tat Transactivation. J. Nat. Prod. 2002, 65 (8), 1091–1095. (63) Bianchi, N.; Rutigliano, C.; Passadore, M.; Tomassetti, M.; Pippo, L.; Mischiati, C.; Feriotto, G.; Gambari, R. Targeting of the HIV-1 Long Terminal Repeat with Chromomycin Potentiates the Inhibitory Effects of a Triplex-Forming

Oligonucleotide on Sp1– DNA Interactions and in Vitro Transcription. Biochem. J. 1997, 326 (3), 919–927.